Efficient synthesis of $BiVO_4$ nanobelts with enhanced visible-light-driven photocatalytic activity for water purification

Yan Li, Zhisheng Wu, Leijun Li, Fei Xing, Cuirong Liu*

School of Material Science and Engineering, Taiyuan University of Science and Technology, Taiyuan 030024, China.

Abstract: $BiVO_4$ powder was synthesized by a simple hydrothermal method. The nanobelts with well dispersed and uniform morphology were synthesized by controlling the temperature. The structure of $BiVO_4$ powder was studied by scanning electron microscopy (SEM) and transmission electron microscopy (TEM). The diameter of the nanobelts was about 50 nm. The structure and composition of the nanobelts were studied by X-ray diffraction (XRD), photoluminescence (PL) and X-ray photoelectron spectroscopy (XPS). The absorption intensity of $BiVO_4$ powder in UV-Vis region was compared by UV–vis diffuse reflectance spectroscopy. As a photocatalyst, $BiVO_4$ nanobelts have good photocatalytic ability under visible light irradiation, which is very useful for the treatment of environmental wastewater. The synthesized nanobelts photocatalyst can be reused without destroying its structure. The reusability and chemical stability of photocatalysts are of great significance for practical application.

Keywords: $BiVO_4$; nanobelts; photocatalyst; reusability; stability.

1. Introduction

In recent years, semiconductor photocatalysts have attracted extensive interest in

* ligang12234@163.com (corresponding author: Cuirong Liu)

the degradation of organic pollutants, which is considered as a feasible and ideal strategy to solve environmental problems. [1-6] Metal oxide semiconductors such as TiO_2 and ZnO are widely used in the field of photocatalysis because of their stable performance and low cost. [7-10] The main disadvantage of these wide band gap semiconductors is that only the ultraviolet region of the spectrum can be effectively utilized. A key goal in this field is to continue to develop semiconductor photocatalysts with the functions of effective light absorption, charge separation and charge transfer. [11, 12] The band gap of $BiVO_4$ is relatively small, and this advantage is considered to be a potential attraction photocatalyst for degrading organic pollutants under visible light irradiation. [13-15] However, the performance of traditional $BiVO_4$ materials is quite different from what people expected.

Many studies have shown that morphological structure is one of the key factors of photocatalytic activity. [16-19] Many nano graphs of $BiVO_4$ materials have been reported in different photocatalytic reactions. [20-23] One-dimensional (1D) $BiVO_4$ nanostructure facilitates the transport of charge along the 1D geometry and the separation of charge across a large interfacial surface region. [24, 25] The nanobelts $BiVO_4$ have relatively high surface area to volume ratio, which is advantageous in providing a large interfacial contact area between the photocatalyst and the reactant, thus enhancing the photocatalytic performance of the catalyst. [26] There are many ways to synthesize $BiVO_4$ nanobelts, such as, sol-gel, electrospinning and so on. [27, 28] Some progress has been made in the preparation of $BiVO_4$ nanobelts. However, it remains a challenge for the synthesis of $BiVO_4$ nanobelts with high purity and

controlled structure. The current synthesis method is increasingly inclined to environmental friendly methods. [29-32]

Herein, no surfactant and doped hydrothermal methods are used to synthesize pure $BiVO_4$. $BiVO_4$ with different morphologies was synthesized by controlling the temperature of hydrothermal method. The $BiVO_4$ nanobelts with large surface area and enhanced photocatalytic activity were selected by instrumental analysis, and its photocatalytic performance was the best. The reusability and chemical stability of $BiVO_4$ nanobelts have also been studied.

2. Experimental section

2.1 Synthesis of $BiVO_4$ nanostructures

Typically, 2 mmol of $Bi(NO_3)_3 \cdot 5H_2O$ was dissolved in 20 mL of water and ethanol mixture (20 ml) (water: ethanol of 1:2) to form solution A. Secondly, 2 mmol of NH_4VO_3 was dissolved in water and ethanol mixture (20 ml) (water: ethanol of 1:2) to form solution B. Then, solution A was dropwise added into solution B in ten minutes. After mixing the two solutions, the Yellow precipitation was obviously precipitated. The pH value of the obtained suspension was adjusted to 7 using NaOH solution, and then the mixed solution was stirred vigorously for 1 hour. Prepare four copies of this mixed solution. Then, the four mixed solutions of the mixture were moved to Teflon-lined stainless steel autoclave separately. The four sealed autoclaves are kept at 140, 160, 180 and 200℃for 24 hours separately and then cooled down to room temperature. When the solution cooled down to room temperature, the precipitation was separated by a filter. The precipitation was repeatedly cleaned by

ultrapure water and anhydrous ethanol. Then it is dried in a vacuum oven at 60 ℃ for 12 hours. The obtained samples were named by the temperature as $BiVO_4$ (temperature).

2.2 Photocatalytic activities

A 30 mg sample was added to the RhB aqueous solution and continuously stirred for 30 minutes in the absence of light to achieve the dye adsorption-desorption equilibrium. The entire experiment was carried out at room temperature. Then the solution was irradiated by a 300 W Xe lamp equipped with a wave filter plate (λ>420 nm) and stirred continuously. During the irradiation, samples were taken every 10 minutes and the catalyst was removed by centrifugation. Finally, the RhB solution concentration was measured using the UV-visible spectrophotometers.

2.3 Characterization

The samples were characterized with X-ray powder diffraction (XRD, rigakud/max-2550, Japan), Raman spectrometer (Finder Insight Pro, China), scanning electron microscopy (SEM, Prisma E) , transmission electron microscopy (TEM, HT7820), UV/Vis spectroscope (Hitachi, U-4100) and X-ray photoelectron spectroscopy (XPS, ESCLAB 250).

3. Results and discussion

As shown in Fig.1, the morphologies of $BiVO_4$ prepared at different temperatures were characterized by SEM. Temperature has a great influence on the morphology of $BiVO_4$ samples. It is obviously seen from Fig.1a that the morphology of the product is some irregular nanorods. These disordered nano-morphologies are

inevitably not good for photocatalytic experiments. Fig.1b shows that the morphology of the product is a mixture of nanorods and nanobelts with the temperature at 160℃. When the temperature is 180℃ (Fig.1c), the nanomorphology of $BiVO_4$ samples is very regular. The diameter of these nanobelts is about 50 nm. Such regular nano-morphology is conducive to the development of photocatalytic experiments, and will certainly have excellent experimental results. As the temperature rises to 200℃ (Fig.1d), the diameter of the nanobelts gradually increases to more than 200 nm and the morphology gradually grows into the shape of bamboo leaves. It seems that the temperature of hydrothermal method must be controlled at 180 ℃ in order to obtain good nano-morphology.

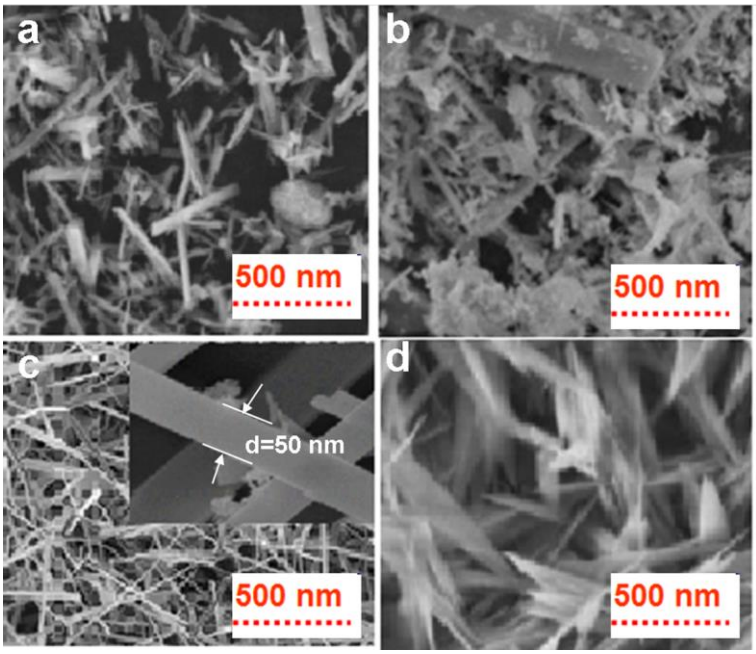

Fig.1. SEM images of $BiVO_4$ samples produced at temperature 140℃ (a), 160 ℃ (b), 180℃ (c), 200℃ (d).

Fig.2 shows the diffuse reflectance spectra of $BiVO_4$ nano-samples prepared with four different temperatures in the range of 400-750 nm. With the increasing

temperature, the absorption of the sample in the visible region also increases, while at 180 ℃ the absorption is the best. This good visible absorption property is mainly due to the electron transition from mixed Bi-O valence band to V conduction band. [33] The results show that the nanobelts prepared at this temperature are conducive to the photocatalytic experiment.

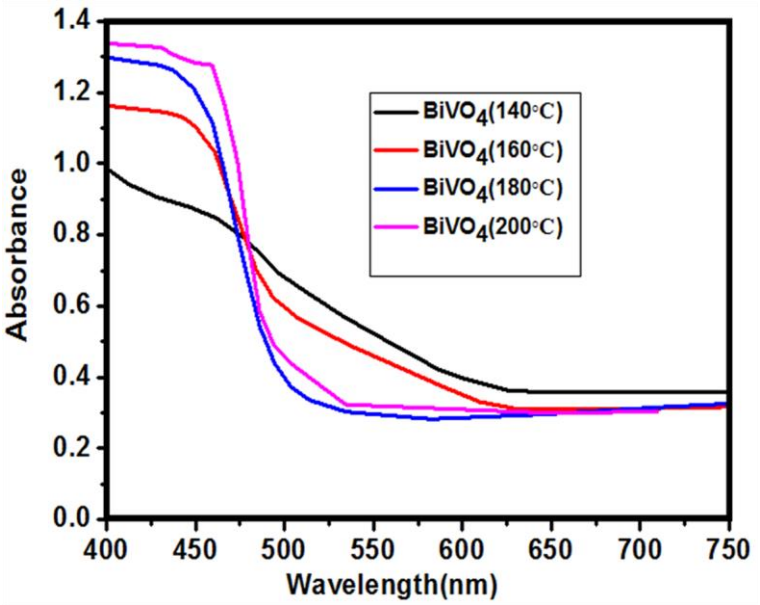

Fig.2. UV-vis diffuse reflectance spectra of $BiVO_4$, with temperature of 140, 160, 180 and 200 ℃.

The chemical composition of the appropriate $BiVO_4$ nanobelts was confirmed by EDS. As can be seen from Fig.3a, $BiVO_4$ consists of Bi, V, and O elements. A small amount of C and Cu element signals come from copper grids. The crystallinity and phase structure of $BiVO_4$ powder synthesized by hydrothermal method at different temperatures were studied by XRD and the results are shown in Fig.3b. All diffraction peaks at different temperature can be well indexed to monoclinic $BiVO_4$. There were no impure peaks were found in the samples. This

indicates that the sample obtained by the experimental reaction is pure and has no other residue. All diffraction peaks of $BiVO_4$ samples conform to (101), (011), (112), (004), (200), (020), (204) and (024) planes, which are consistent with the PDF standard card of $BiVO_4$ (JCPDS, No. 75-2480). When the experimental temperature is controlled at 180, the diffraction peaks are sharper than those at other temperatures, indicating that the products are highly crystallized at this temperature. The raman spectra of $BiVO_4$ nanobelts was shown in Fig.3c. The classical vibration bands of $BiVO_4$ can be clearly seen in the figure. Raman bands of 326, 369, 719 and 828 cm^{-1} can be observed. The Raman bands at 719 and 828 cm^{-1} are attributed to two different stretching modes of V-O bonds, which belong to the antisymmetric and symmetric stretching mode of VO_4 tetrahedron. The peaks at 328 and 369 cm^{-1} are attributed to the bending mode of VO_4 tetrahedron. All these peaks of raman spectra not only prove that they are consistent with the vibration mode of monoclinic scheelite VO_4, but also further prove that the products obtained are pure.

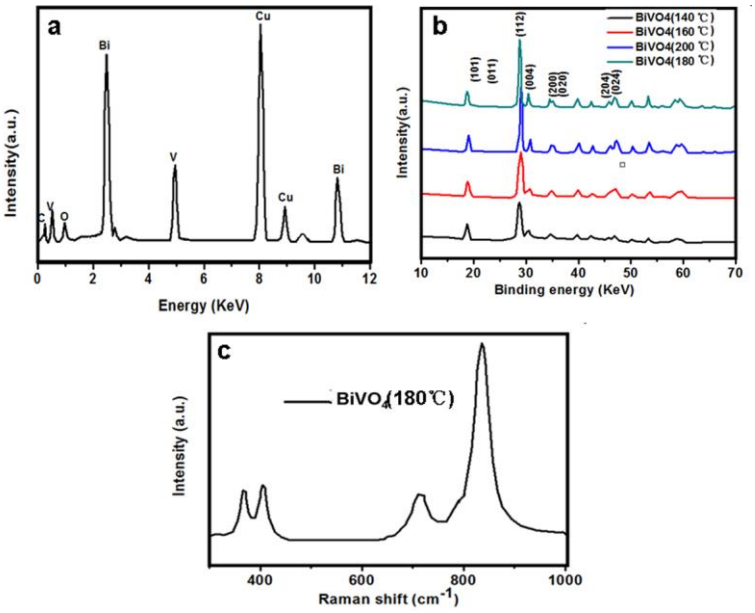

Fig.3. (a) EDS spectrum of $BiVO_4$ (180℃), (b) XRD pattern of the different temperature products of Samples, (c) Raman spectra of $BiVO_4$ (180℃).

In order to further reveal the morphological and structural information of the $BiVO_4$ (180℃) nanobelts, the $BiVO_4$ nanobelts were analyzed by TEM, as shown in Fig.4. Apparently, all of the as-prepared samples were formed in nanobelts. It can be found from Fig. 4a and b that the nanobelts are well dispersed and their diameters are the same as those obtained by SEM. The distance between two sets of neighboring fringes which measured 0.308 nm is responding to the (112) plane distance of monoclinic $BiVO_4$ (Fig. 4d). It is in good agreement with the above XRD results.

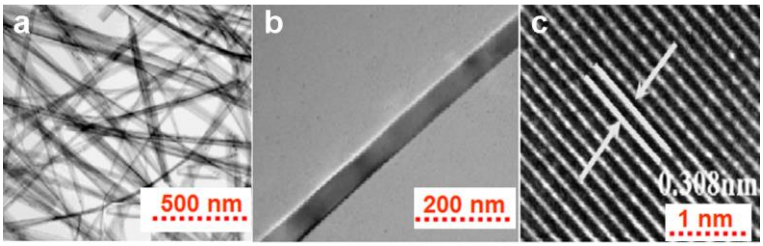

Fig.4. TEM (a, b) and HRTEM (c) images of the as-prepared BiVO4 nanobelts.

The chemical composition of the product was studied by XPS. Fig.5a shows all the XPS spectra of $BiVO_4$, which Bi, O and V elements can be studied. Fig. 3b-d shows the high resolution spectra of Bi4f, V2p, O1s and $BiVO_4$ composites, respectively. As shown in Fig. 5b, Bi $4f_{7/2}$ and Bi $4f_{5/2}$ were observed at 164.2 eV and 160.1 eV, respectively. Fig. 5c shows a peak at 529.8eV, which originates from V 2p.The existence of energy binding peaks at 530.5 eV is attributed to oxygen in $BiOV_4$ nanobelts. [34, 35]

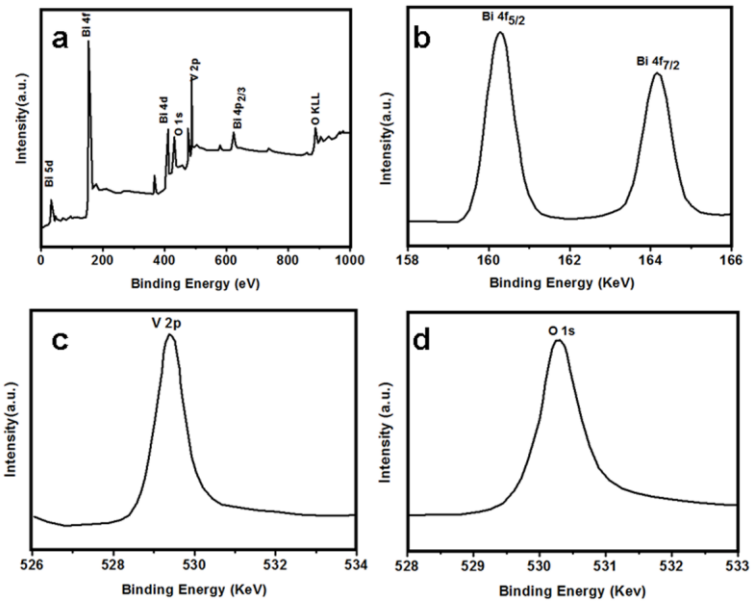

Fig.5. Typical XPS survey spectra of BiVO4(a) and high resolution XPS spectrum of Bi 4f (b), V 2p (c), O 1s (d).

The time evolution diagram of ultraviolet-visible spectra (Fig.6a.) clearly shows that the absorption spectra of $BiVO_4$ samples can degradate the RhB. It can be found from the spectra that all absorption peaks of RhB aqueous solution start at 553. With the prolongation of irradiation time, the absorption wavelength gradually decreases and changes to a shorter wavelength. The chromogenic group of the dye has been destroyed. The photocatalytic activity of the samples prepared at different temperature was also studied. As can be seen from the Fig.6b, $BiVO_4$ nanomaterials prepared with different temperature can degrade RhB. However, photocatalysts prepared at 180℃ can almost completely degrade RhB, while other catalysts can not. In addition, the blank experiment proved that the self-photolysis of RhB could be neglected. The results showed that the photocatalytic degradation efficiency of $BiVO_4$ (180℃) was

significantly higher than that of other photocatalysts. It indicates that the photocatalyst prepared at 180 ℃had good photocatalytic activity.

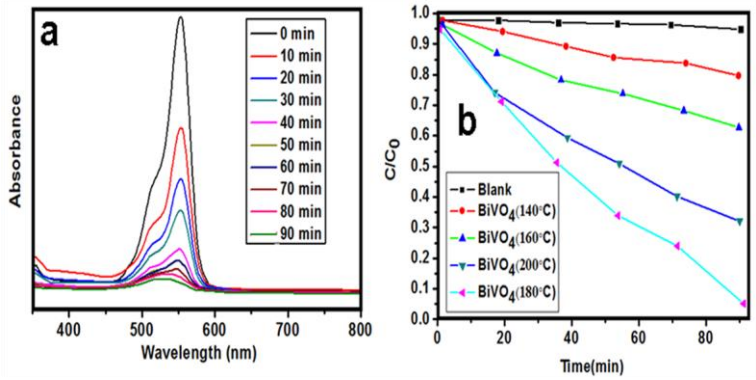

Fig.6. (a) Absorption spectra of RhB solution in the presence of BiVO4 (180℃) photocatalyst, (b) Degradation of RhB by different photocatalysts under visible light irradiation.

The reusability and chemical stability of photocatalysts are of great significance for practical application. Good stability and reusability are the affirmation of the experimental products. It means that a great opportunity for products to invest in real life to control water pollution can be achieved. Fig. 7a shows that the catalytic performance of the catalyst remains stable after five times of reuse. The crystal structure of the product remains unchanged before and after catalysis, indicating that the catalytic process will not break the internal structure of the catalyst (Fig.7b). This can support why the catalytic performance of the catalyst remains stable after repeated use.

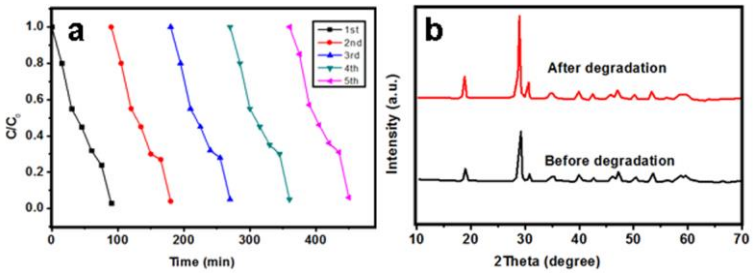

Fig.7. BiVO4 was used to retrieve RhB under visible light. (b) XRD images before and after five runs.

In order to understand the main active substances of RhB degradation in the catalytic reaction process and to explore its reaction mechanism, three catalysts, 1,4-benzoquinone (BQ), ammonium oxalate (AO) and tert-butanol (t-BuOH), were used to study hydroxyl radical (OH^-), pore (h^+) and superoxide groups(O_2^-). The degradation rate of MB by $BiVO_4$ (180 °C) decreased significantly after adding AO as hole (h+) scavenger in the solution, indicating that hole participated in the degradation of MB. The degradation rate of RhB decreased slightly when BQ was added to the solution as oxygen scavenger. This indicates that there is no superoxide radical (O_2^-) in the degradation process of MB. However, with the addition of OH^- scavenger (t-BuOH), the degradation of RhB decreased significantly, which indicated that OH^- played an important role in the degradation of RhB (Fig.8.).

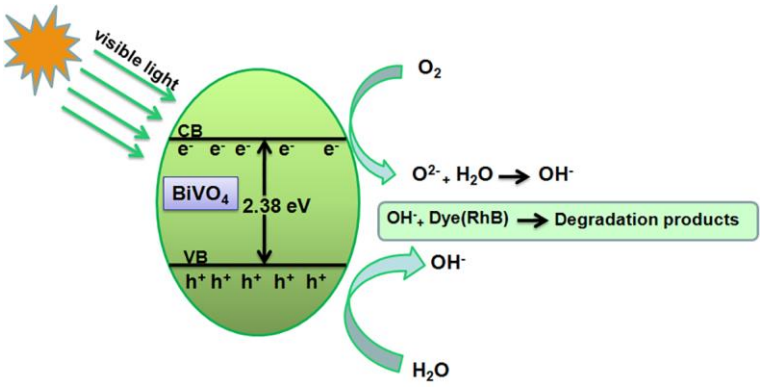

Fig.8. The mechanism of the BiVO4 (180°C) nanobelts for the degradation of RhB.

4. Conclusion

In this study, $BiVO_4$ nanobelts were synthesized without adding any surfactants. The width of the nanobelts is about 50 nm. In the visible region, the prepared $BiVO_4$ nanobelts exhibit excellent absorption and good photocatalytic reaction during RhB degradation, which may be attributed to their unique morphology. Nanobelts have uniform nanostructure and high purity morphology. Compared with traditional nanobelts, their photocatalytic and photocatalytic properties have been greatly improved, which has broad application prospects in environmental treatment and energy conversion.

Acknowledgments

This work was financially supported by National Natural Science Foundation of China (51875384), Taiyuan University of Science and Technology Ph.D. Startup Fund (20182041), the Fund for Shanxi“1331Project” and Collaborative Innovation Center of Internet+3D Printing in Shanxi Province（CiCi3DP).

References

[1] Jiang Z.; Wei W.; Mao, D.; Chen, C. ; Shi, Y. ; Lv, X.; Xie, J. Silver-loaded nitrogen-doped yolk–shell mesoporous TiO_2 hollow microspheres with enhanced visible light photocatalytic activity. *Nanoscale* **2015**, 7, 784-797.

[2] Liu, B.; Nakata, K.; Sakai, M.; Saito, H.; Ochiai, T.; Murakami, T. ; Fujishima, A. Mesoporous TiO_2 core–shell spheres composed of nanocrystals with exposed

high-energy facets: facile synthesis and formation mechanism. Langmuir **2011**, 27,8500-8508.

[3] Xuan, S.; Jiang, W.; Gong, X.; Hu, Y.; Chen, Z. Magnetically separable Fe_3O_4/TiO_2 hollow spheres: fabrication and photocatalytic activity. J. Phys. Chem. C **2008**, 113, 553-558.

[4] Deng, Q.; Duan, X.; Ng, D. H.; Tang, H.; Yang, Y.; Kong, M.; Wang, G. Ag nanoparticle decorated nanoporous ZnO microrods and their enhanced photocatalytic activities. ACS Appl. Mater. Interfaces **2012**, 4, 6030-6037.

[5] Wang, H.; Zhang, L; Chen, Z.; Hu, J.; Li, S.; Wang, Z.; Wang, X. Semiconductor heterojunction photocatalysts: design, construction, and photocatalytic performances. Chem. Soc. Rev. **2014** ,43, 5234-5244.

[6] Marschall, R. Semiconductor composites: strategies for enhancing charge carrier separation to improve photocatalytic activity. Adv. Funct. Mater. **2014**, 24, 2421-2440.

[7] Shang, S.; Jiao, X.; Chen, D. Template-free fabrication of TiO_2 hollow spheres and their photocatalytic properties. ACS Appl. Mater. Interfaces **2012**, 4, 860-865.

[8] Lv, K.; Cheng, B.; Yu, J.; Liu, G. Fluorine ions-mediated morphology control of anatase TiO_2 with enhanced photocatalytic activity. Phys. Chem. Chem. Phys. **2012**,14, 5349-5362.

[9] Fan, F.; Feng, Y.; Tang, P.; Li, D. Facile synthesis and photocatalytic performance of ZnO nanoparticles self-assembled spherical aggregates. Mater. Lett. **2015**, 158, 290-294.

[10] Luo, Q. P.; Yu, X. Y.; Lei, B. X.; Chen, H. Y.; Kuang, D. B.; Su, C. Y. Reduced graphene oxide-hierarchical ZnO hollow sphere composites with enhanced photocurrent and photocatalytic activity. J. Phys. Chem. C **2012**, 116, 8111-8117.

[11] Zheng, L.; Han, S.; Liu, H.; Yu, P.; Fang, X. Hierarchical MoS_2 nanosheet@TiO_2 nanotube array composites with enhanced photocatalytic and photocurrent performances. Small **2016**, 12, 1527-1536.

[12] Liu, S.; Zheng, L.; Yu, P.; Han, S.; Fang, X. Novel composites of α‐Fe_2O_3 tetrakaidecahedron and graphene oxide as an effective photoelectrode with enhanced photocurrent performances. Adv. Funct. Mater. 26 (2016) 3331-3339.

[13] Li, R.; Han, H.; Zhang, F.; Wang, D.; Li, C. Highly Efficient Photocatalysts Constructed by Rational Assembly of Dual-Cocatalysts Separately on Different Facets of $BiVO_4$. Energy Environ. Sci. **2014**, 7, 1369-1376.

[14] Iwase, A.; Kudo, A. Photoelectrochemical water splitting using visible-light-responsive $BiVO_4$ fine particles prepared in an aqueous acetic acid solution . J. Mater. Chem. **2010**, 20, 7536-7542.

[15] Li, Y.; Xiao, X.; Ye, Z. Facile fabrication of tetragonal scheelite (ts) $BiVO_4$/g-C_3N_4 composites with enhanced photocatalytic performance. Ceram. Int. **2018**, 44, 7067-7076.

[16] Lin, B.; Xue, C.; Yan, X.; Yang, G.; Yang, B. Facile fabrication of novel SiO_2/g-C_3N_4 core–shell nanosphere photocatalysts with enhanced visible light activity. Appl. Surf. Sci **2015**, 357, 346-355.

[17] Lin, D.; Wu, H.; Zhang, R.; Pan, W. Enhanced photocatalysis of electrospun Ag−ZnO heterostructured nanofibers. Chem. Mat. **2009**, 21, 3479-3484.

[18] Zhang, Z.; Shao, C.; Li, X.; Zhang, L.; Xue, H.; Wang, C.; Liu, Y. Electrospun nanofibers of ZnO−SnO_2 heterojunction with high photocatalytic activity. J. Phys.

Chem. C **2010**, 114, 7920-7925.

[19] Zhang, L.; Wang, H.; Chen, Z.; Wong, P. K.; Liu, J. Bi_2WO_6 micro/nano-structures: synthesis, modifications and visible-light-driven photocatalytic applications. Appl. Catal. B-Environ **201**1, 106, 1-13.

[20] Li, C.; Wang, S.; Wang, T.; Wei, Y. ; Zhang, P.; Gong, J. Monoclinic porous $BiVO_4$ networks decorated by discrete g-C_3N_4 Nano-Islands with tunable coverage for highly efficient Photocatalysis. Small **2014**, 10, 2783-2790.

[21] Shi, W.; Yan, Y.; Yan, X. Microwave-assisted synthesis of nano-scale $BiVO_4$ photocatalysts and their excellent visible-light-driven photocatalytic activity for the degradation of ciprofloxacin. Chem. Eng. J. **2013**, 215, 740-746.

[22] Wang, Z. ; Luo, W.; Yan, S.; Feng, J.; Zhao, Z.; Zhu, Y.; Zou, Z. $BiVO_4$ nano–leaves: Mild synthesis and improved photocatalytic activity for O_2 production under visible light irradiation. CrystEngComm **2011**, 13, 2500-2504.

[23] Sharma, R.; Singh, S.; Verma, A.; Khanuja, M. Visible light induced bactericidal and photocatalytic activity of hydrothermally synthesized $BiVO_4$ nano-octahedrals. J. Photochem. Photobiol. B-Biol. **2016**,162, 266-272.

[24] Cheng, J.; Feng, J.; Pan, W. Enhanced photocatalytic activity in electrospun bismuth vanadate nanofibers with phase junction. ACS Appl. Mater. Interfaces **2015**, 7, 9638-9644.

[25] Jiao, Z.; Yu, H.; Wang, X.; Bi, Y. Ultrathin $BiVO_4$ nanobelts: controllable synthesis and improved photocatalytic oxidation of water. RSC Adv. **2016**, 6, 73136-73139.

[26] Liu, H.; Yang, W.; Wang, L.; Hou, H.; Gao, F. Electrospun $BiVO_4$ nanobelts with tailored structures and their enhanced photocatalytic/photoelectrocatalytic activities. CrystEngComm **2017**, 19, 6252-6258.

[27] Liu, G.; Liu, S.; Lu, Q.; Sun, H.; Xu, F.; Zhao, G. Synthesis of monoclinic $BiVO_4$ microribbons by sol–gel combined with electrospinning process and photocatalytic degradation performances .J. Sol-Gel Sci. Technol. **2014**, 70, 24-32.

[28] Liu, Z.; Lu, Q.; Guo, E.; Liu, S. Electrospinning synthesis of $InVO_4/BiVO_4$ heterostructured nanobelts and their enhanced photocatalytic performance. J. Nanopart. Res. **2016**, 18, 236.

[29] Akir, S.; Barras, A.; Coffinier, Y.; Bououdina, M.; Boukherroub, R.; Omrani, A. D. Eco-friendly synthesis of ZnO nanoparticles with different morphologies and their visible light photocatalytic performance for the degradation of Rhodamine B. Ceram. Int. **2016**, 42, 10259-10265.

[30] Shao, P.; Tian, J.; Shi, W.; Gao, S.; Cui, F. Eco-friendly one-pot synthesis of ultradispersed TiO_2 nanocrystals/graphene nanocomposites with high photocatalytic activity for dye degradation. J. Mater. Chem. A **2015**, 3, 19913-19919.

[31] Iqbal, W.; Dong, C.; Xing, M.; Tan, X.; Zhang, Eco-friendly one-pot synthesis of well-adorned mesoporous g-C_3N_4 with efficiently enhanced visible light photocatalytic activity. J. Catal. Sci. Technol. **2017**, 7, 1726-1734.

[32] Li, Y.; Zhou, J.; Fan, Y.; Ye, Y.; Tang, B. Preparation of environment-friendly 3D eggshell membrane-supported anatase TiO_2 as a reusable photocatalyst for degradation of organic dyes. Chem. Phys. Lett. **2017**, 689, 142-147.

[33] Cooper, J. K.; Gul, S.; Toma, F. M.; Chen, L.; Glans, P.-A. ; Guo, J.; Ager, J. W.; Yano, J.; Sharp, I. D. Electronic Structure of Monoclinic $BiVO_4$. Chem. Mater. **2014**, 26, 5365-5373.

[34] Xie, M.; Zhang, Z.; Han, W.; Cheng, X.; Li, X.; Xie, E. Efficient hydrogen evolution under visible light irradiation over $BiVO_4$ quantum dot decorated screw-like SnO_2 nanostructures. J. Mater. Chem. A **2017**, 5, 10338-10346.

[35] Cheng, J.; Yan, X.; Mo, Q. ; Liu, B.; Wang, J.; Yang, X.; Li, L. Facile synthesis of g-C_3N_4/$BiVO_4$ heterojunctions with enhanced visible light photocatalytic performance. Ceram. Int. **2017**, 43, 301-307.